ADVANCED ELECTRONIC MATERIALS
Open Access
www.advelectronicmat.de

Orthogonal-Stacking Integration of Highly Conductive Silicide Nanowire Network as Flexible and Transparent Thin Films

Rongrong Yuan, Wentao Qian, Ying Zhang, Zongguang Liu, Junzhuan Wang, Jun Xu, Kunji Chen, and Linwei Yu**

Flexible and transparent conductive (FTC) thin films are indispensable elements in building high-performance flexible or soft electronics and displays. Slim inorganic nanowires (NWs), with excellent conductivity and durability, are ideal one-dimensional ingredients to weave a quasi-continuous FTC network. However, a precise spatial arrangement of these ultrathin NWs, to form an optimal interconnected network, represents still a difficult challenge. In this work, a catalytic growth of orderly SiNW arrays, via an in-plane solid-liquid-solid mechanism, and an orthogonal-stacking integration of the SiNWs into a 2-layer cross-linked network, followed by a direct alloy formation and soldering of highly conductive SiNi alloy NWs upon a flexible polyimide polymer, is demonstrated. It is also shown that the flexibility of the SiNi FTC network can be significantly enhanced with an elastic spring design of the silicide NW channels, leading to an impressive transmittance of ≈90%, a moderately equivalent sheet resistance of 130 Ω sq^{-1} and a durable flexibility that can sustain repetitive bending to a 2 mm radius for >1000 cycles. These results highlight the unique capabilities of an optimal spatial arrangement, precise assembly/soldering and elastic geometry design of alloy NWs to enable a new generation of high-performance FTC thin film material for future flexible electronics, displays, and bio-interfaced sensors.

1. Introductions

In the last decade, the implementation of flexible electronics and displays are gaining more and more momentum, where an essential component for all the foldable or deformable displays,[1] wearable electronics,[2,3] skin/tissue-interfaced sensors[4–6], and monitors[7] is the flexible, transparent, and conductive thin film (FTC-TF) electrodes, which are supposed to sustain large bending, for example to a small radius of <3 mm,[8] durable in ambient environment and suitable for high-density integration of individual light emission diode (LED), logic or sensing units over flexible polymer substrates, as schematically diagrammed in **Figure 1**a. To this end, conductive organic materials have been first explored as flexible electrodes,[9] but usually suffer from the problems of relatively low conductivity[10] and quick deterioration in prolonged air exposure.[11] On the other hand, the commonly used transparent conductive oxide (TCO) material of indium tin oxide (ITO) in flat-panel displays[12] and solar cells[13] are very stable, transparent and conductive,[14–16] but is unfortunately brittle and prone to crack even under slight bending (with local strain <1%),[17] which greatly limits its applications in flexible and stretchable electronics.

Recently, inorganic nanostructured materials, such as graphene,[18] carbon nanotubes,[6,19] metallic nanowires (NWs)/film,[20–23] have been heavily investigated for FTC-TF applications, as they are more adaptive to the large strains under bending or stretching. Usually, multilayers of the carbon or metallic NWs need to deposited, spin-coated or stacked to form a quasi-continuous cross-linked percolative networks. For example, stacking number of $N_{stk} \geq 5$, for CNT or silver (Ag) NW constituents,[6,24] are typically needed to ensure a reasonable conductivity. This is because the randomly distributed NWs are loosely crossed to each other, and the stochastic crossing-contacts usually account for a large portion of the high overall thin film resistance, as well as the structural/electrical instability under distortions. Importantly, if the NW density is not high enough, a high electric conductivity fluctuation will arise in the random percolative network, particularly for the shorter interconnect distance in high density integration.[25,26] Though adding more stacking layers can help to alleviate this issue, this has to be traded-off against the transparency of the FTC-TF.

R. Yuan, W. Qian, Y. Zhang, Z. Liu, J. Wang, J. Xu, K. Chen, L. Yu
National Laboratory of Solid-State Microstructures/School of Electronic Science and Engineering, Nanjing University
Collaborative Innovation Center of Advanced Microstructures
Nanjing 210093, China
E-mail: liuzongguang@nju.edu.cn; yulinwei@nju.edu.cn

The ORCID identification number(s) for the author(s) of this article can be found under https://doi.org/10.1002/aelm.202201185.

© 2023 The Authors. Advanced Electronic Materials published by Wiley-VCH GmbH. This is an open access article under the terms of the Creative Commons Attribution License, which permits use, distribution and reproduction in any medium, provided the original work is properly cited.

DOI: 10.1002/aelm.202201185

ADVANCED ELECTRONIC MATERIALS
Open Access
www.advelectronicmat.de

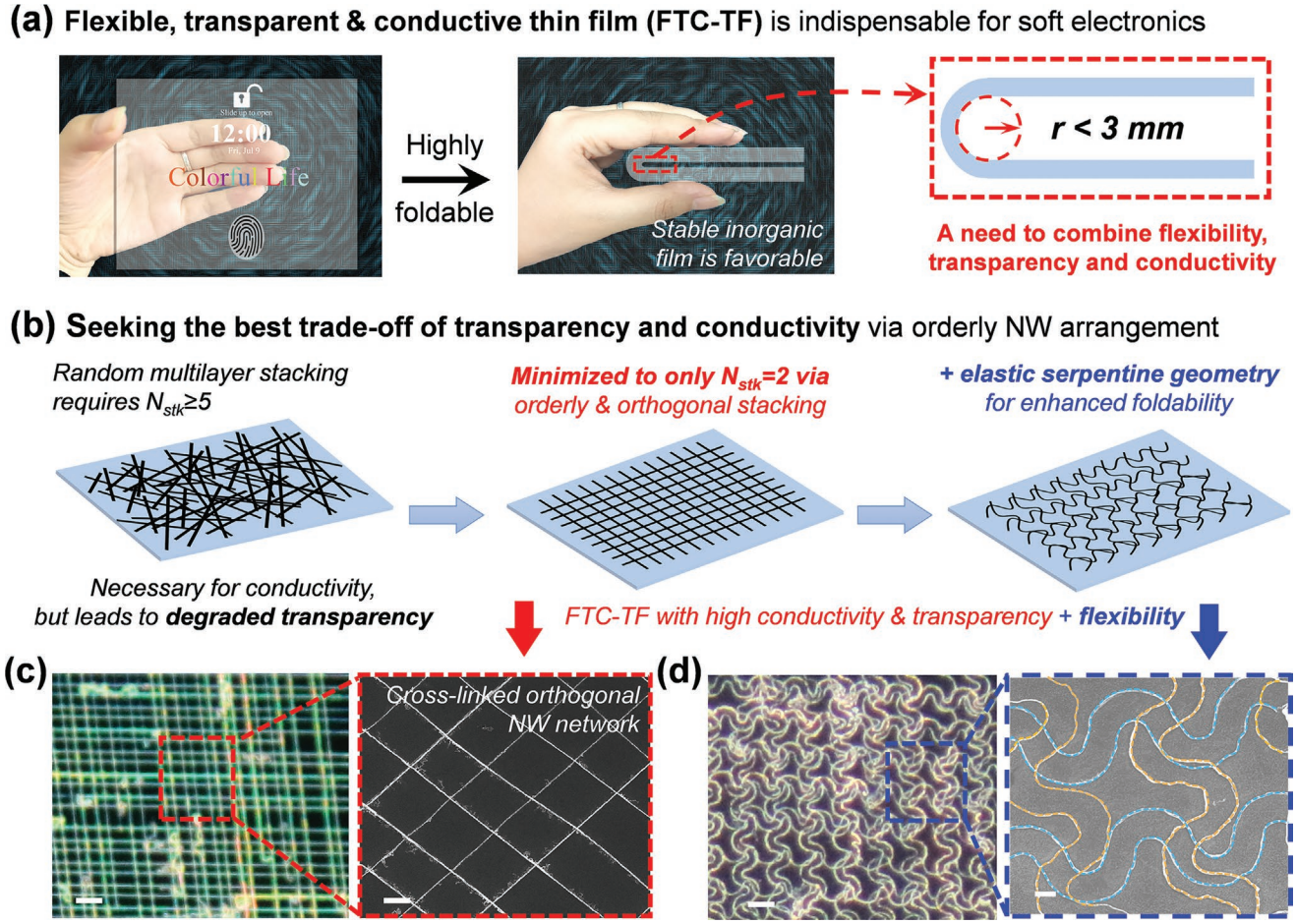


Figure 1. a) Flexible and transparent electrodes are indispensable component for transparent folding electronics, where many foldable applications demand a bending radius as small as 3 mm. b) Weaving orderly NW network via guided growth and reliable 2-layer transferring and crossing, plus elastic geometry, is the key to fabricate ideal FTC thin film with the minimal stacking layer while achieving sufficient conductivity and transparency. The optical (left) and SEM (right) images of the mutual crossed c) straight and d) spring-shaped Si NWs. Scale bars in the left and the right panels of (c) are of 5 and 2 µm, while those in (d) are of 10 and 5 µm, respectively.

Actually, in an ideal NW-woven network, every single constituent NW should be best used, that's placed only in the necessary place to guarantee a sufficient conductivity of a quasi-continuous network, with the minimal stacking number of N_{stk} = 2, while leaving as large as possible space among the NWs to maximize the overall transparency. In addition, extra flexibility of the NW-formed FTC network can be derived from an elastic shape design of the NW ingredients, as depicted in Figure 1b. A properly-designed and integrated NW network, with the minimal stacking layer and slim diameter much smaller than the visible wavelengths, could enable a new generation of high-performance FTC-TF material that has not been demonstrated so far, particularly for fabrication via a scalable and low-cost growth integration or designable NW-weaving approach.

In this work, we first explore a guided growth of regular array of ultralong SiNWs, via an in-plane solid-liquid-solid (IPSLS) mechanism established in our previous works,[27–33] which can be reliably transferred and cross-stacked upon flexible polyimide (PI) films to weave a quasi-continuous network with designable orthogonal-stacking layout that guarantees simultaneously a continuous conductive pathway of crossed NWs and a high overall transparency. To enhance the conductivity of the network, the SiNWs on PI substrate were coated with Ni thin film and annealed at 350 °C to transform into highly conductive SiNi alloy NWs, which are directly connected to each other at the crossing points, without the use of any other metal electrodes. The SiNi-NWs can also be designed to be straight or of spring wavy forms (see Figure 1c,d), indicating an extra means to boost the flexibility or bendability of the alloy NW-weaving FTC network.

2. Results and Discussion

The orderly SiNW or silicon nano spring (SiNS) array were first grown on SiO_2/wafer substrate, led by indium (In) catalyst droplets following the guiding edges pre-patterned by using lithography and reactive ion etching (RIE), via an IPSLS growth strategy.[27–33] In contrast to the conventional gas-feeding vapor-liquid-solid (VLS) growth mode,[34,35] a thin layer of amorphous silicon (a-Si) was deposited by using PECVD on the whole

© 2023 The Authors. Advanced Electronic Materials published by Wiley-VCH GmbH

2199160x, 2023, 7, Downloaded from https://advanced.onlinelibrary.wiley.com/doi/10.1002/aelm.202201185 by Nanjing University, Wiley Online Library on [04/11/2026]. See the Terms and Conditions (https://onlinelibrary.wiley.com/terms-and-conditions) on Wiley Online Library for rules of use; OA articles are governed by the applicable Creative Commons License

ADVANCED ELECTRONIC MATERIALS
Open Access
www.advelectronicmat.de

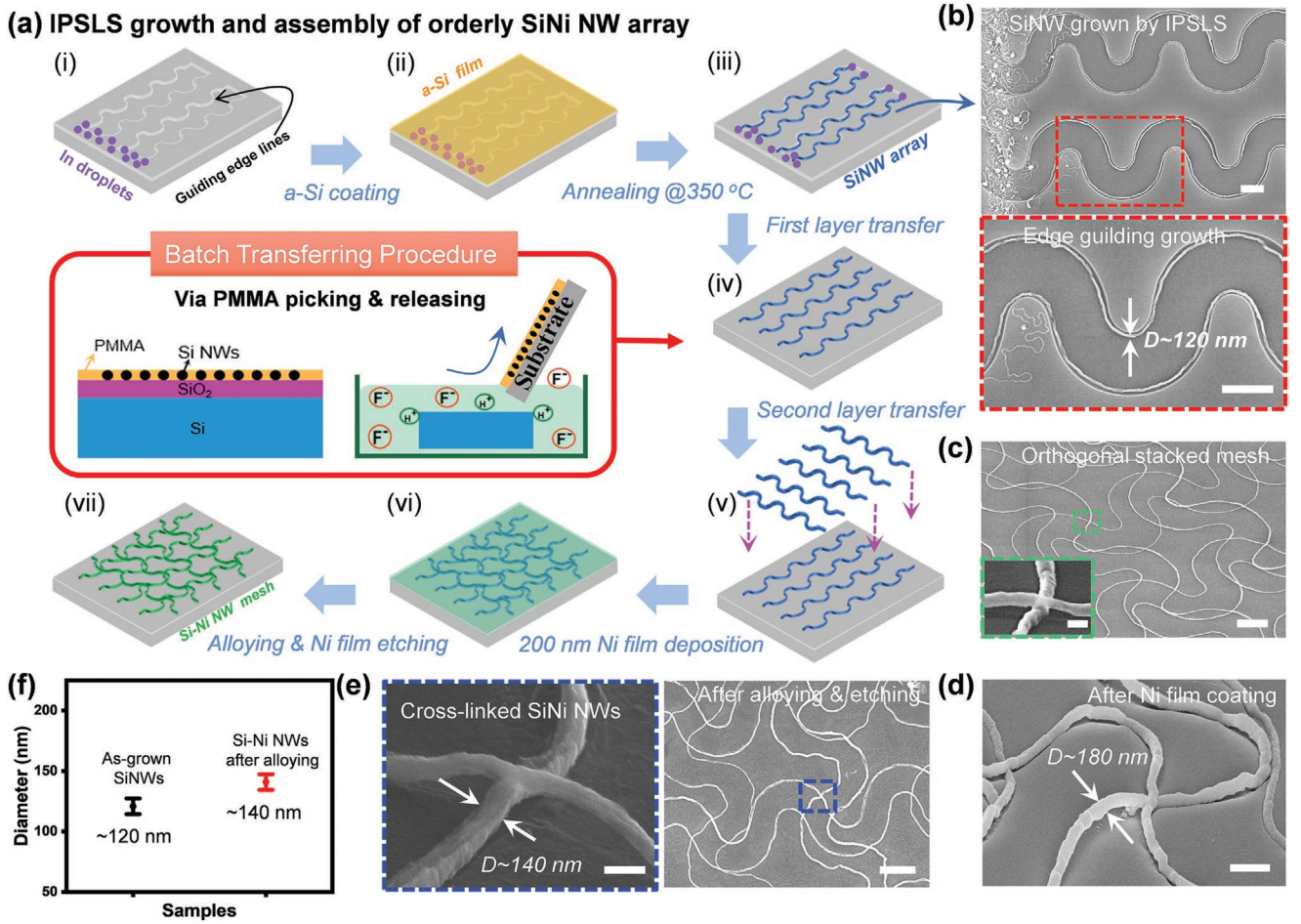


Figure 2. a) The fabrication flow chart of a typical guided IPSLS growth of spring-shaped SiNWs i–iii), the transferring and crossing of the first and the second SiNW layers iv,v), and the nickel film deposition, alloy annealing formation and remnant etching off vi,vii). The PMMA-picking and releasing transferring procedure is illustrated schematically in the middle-inset panel. b) The SEM images of the as-grown SiNWs, and c) the as-transferred crossed SiNW spring network, with an inset showing the crossing point of two SiNWs. d) SiNW network with 200 nm nickel coating. e) show the crossed and joint SiNi NWs, formed after annealing alloy formation and remnant etching. f) statistics of the diameters of the SiNWs before and after the alloy formation step, indicating that the diameter has increased from 120 to 140 nm. Scale bars in the panels of (b) are for 3 µm, (c) for 3 µm (in inset for 100 nm), (d) for 1 µm and (e) for 4 and 200 nm in the right and left panels.

surface as solid precursor medium, which was absorbed by the surface running In droplets to produce crystalline SiNWs along their moving course following the guiding edge lines, as diagrammed in (**Figure 2**a(i–iii)). For instance, the SEM images in Figure 2b show a rather stable guided growth of the IPSLS SiNW along the wavy step edges, with a mean diameter of D_{nw} = 120 nm ± 11 nm according to the statistics. After the growth of SiNWs, the remnant a-Si layer was selectively etched off by H_2 plasma at 120 °C, leaving only an orderly array of crystalline SiNWs.

After that, the SiNWs were first coated by a thin PMMA film (400 nm thick), followed by an under-etching of the sacrificial SiO_2 layer in a diluted HF solution to release the SiNWs/PMMA. Then, the floating PMMA film with embedded SiNWs in solution was picked up and placed onto a foreign PI acceptor substrate, via a procedure as depicted schematically in the central panel of Transfer Procedures in Figure 2a. In the next step, the carrying PMMA layer was dissolved by acetone, followed by a baking at 100 °C, enhance the affinity of the SiNWs to the PI substrate surface (125 µm thick). The same procedure can be repeated safely again, to place the second layer of SiNW array upon the same PI structure, without distortion of the position and ordering of the SiNWs in the first layer (Figure 2a(iv)).

During the placing of the second layer, the orientation of the SiNW array was rotated 90 Degree with respect to the first layer (Figure 2a(v)) to have an orthogonal crossing stacking of the SiNWs, which represents arguably the most efficient and economic arrangement to form a continuous network with the least use of SiNWs. For examples, the optical microscope and SEM images of the orthogonal-stacked networks, consisting of straight SiNWs or SiNSs, are presented in Figure 1c,d, respectively. It is remarkable that, both the orientation and the spacing of the ultra-long SiNWs and SiNSs, with typical length and diameter of 500 and 120 nm (see Figure 2b), can be exactly copied by the solution transferring process. As shown in the enlarged SEM examination of the regular crossing points in Figure 2c, the stacked SiNWs are already closely contacted to each other, linked most likely by van de Waals instead of

© 2023 The Authors. Advanced Electronic Materials published by Wiley-VCH GmbH

2199160x, 2023, 7, Downloaded from https://advanced.onlinelibrary.wiley.com/doi/10.1002/aelm.202201185 by Nanjing University, Wiley Online Library on [04/11/2026]. See the Terms and Conditions (https://onlinelibrary.wiley.com/terms-and-conditions) on Wiley Online Library for rules of use; OA articles are governed by the applicable Creative Commons License

ADVANCED ELECTRONIC MATERIALS
Open Access
www.advelectronicmat.de

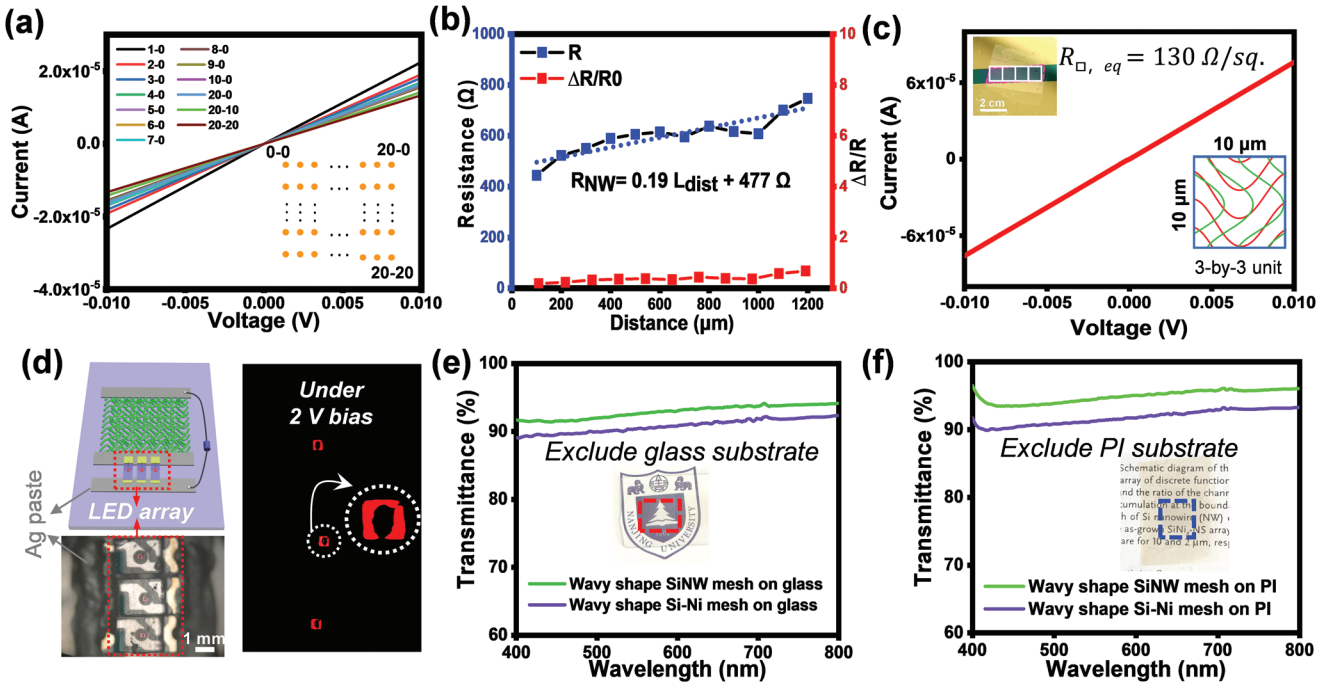


Figure 3. a) The I–V characteristics measured between the electrode pads in an orderly array with different grid separation (0–20), while the resistances and variations were extracted and displayed in b). c) The calculated equivalent sheet resistance of the quasi-continuous NW network, with an inset showing the NW layout within a unit space. d) shows the electric driving of 3 LED units, under 2 V voltage bias, connected by using the NW network as electrodes, with a photo image inset of 3 LEDs in "ON" state. The relative transmittance of SiNWs (green) or alloyed Si-Ni NW (purple) meshes, excluded the glass and PI (12.5 μm) substrates are presented in e) and f), respectively.

chemical bonding force (as the crossly placed SiNWs can still be separated by using tungsten probe equipped in SEM system, though not shown here), which provides a beneficial basis for the subsequent formation of interconnected SiNW network.

After forming the crossing SiNW network, a thin film of 200 nm nickel (Ni) was deposited over the whole sample, by using magnetron enhanced plasma sputtering. As seen in the close SEM examination shown in Figure 2d, the Ni film can indeed wrap over the SiNWs and join them at the crossing places. After annealing at 350 °C in vacuum for 5 min, the Ni capping layer and the SiNWs will inter-diffuse to form SiNi alloy, while the remnant Ni film in the spare regions was etched off selectively by a mixed acid solution (Figure 2a(vii)), see Experimental Section/Methods for more details). The SEM images of the as-formed SiNi-NWs network are presented in Figure 2e, where it is found that 1) the overall layout of the NW or NS network can be well preserved, while the alloy NWs seem to enlarge slightly from $D_{\mathrm{SiNW}} = 120\ nm \pm 11\ nm$ to $D_{NW}^{alloy} = 140\ nm \pm 15\ nm$, according to the statistics in Figure 2f, due to the incorporation of extra Ni atoms into the SiNW to form crystalline alloy phase of $Si_{12}Ni_{31}$ (see Figure S1, Supporting Information) for the TEM analysis, consistent to that found in our previous work.[36]); 2) the inter-diffusion of Si and Ni atoms during the alloy forming process seems to solder the crossing NWs at the joining places, as witnessed in a close SEM scrutiny in Figure 2e, which is a beneficial factor to enhance the overall conductivity, continuity and mechanical stability of the SiNi-NW network. It is also noteworthy that the guided growth of IPSLS SiNW requires only a-Si coating as precursor, which is really low-cost, scalable and compatible to the established large area thin film technology upon glasses substrate or flexible PI film. The conductivity of the SiNi-NS network was first characterized by preparing an array of round Ti (5 nm)/Au (80 nm) electrodes, with diameter and pitch both of 100 μm, deposited by using e-beam evaporation through stainless shadow masks. The current–voltage (I–V) measurements between the electrode pairs with different grid separation, denoted by grid-number (X, Y) with respect to the original one of (0, 0), are plotted in **Figure 3**a. It was found that an excellent Ohmic contact to the SiNi-NS network has been achieved, while the increased separation distance (up to 20 grid) leads to slight decrease in the transport current.

The evolution of the measured resistance against the increased distance, ranging from 100 to 1200 μm, has been extracted and presented in Figure 3b, which can be fitted by linear scaling law of

$$R_{\mathrm{nw}} = (0.19\mathrm{L}_{\mathrm{dist}} + 477)\Omega \quad (1)$$

Indicating a quasi-uniform connectivity of the cross-linked alloy network. In order to extract the equivalent sheet resistance of this SiNi-NS network, a larger region of the network, with width and separation of 4 and 1 cm respectively, was connected by a pair of parallel electrode bars, as depicted in Figure 3c. The measured each sheet resistance of the square NW network is estimated to be 500 Ω sq.$^{-1}$ Considering the actual length and width of the SiNi NWs, within a 3-by-3 unit (see the inset of Figure 3c), the equivalent sheet square is calculated to 130 Ω sq.$^{-1}$ according to the following formulas

$$\mathrm{R}_{\mathrm{sheet,\,eq}} = \eta\, R_{\mathrm{sheet}} = \left(\mathrm{S}_{\mathrm{nw}}/\mathrm{S}_{\mathrm{square}}\right) R_{\mathrm{sheet}} \quad (2)$$

© 2023 The Authors. Advanced Electronic Materials published by Wiley-VCH GmbH

2199160x, 2023, 7, Downloaded from https://advanced.onlinelibrary.wiley.com/doi/10.1002/aelm.202201185 by Nanjing University, Wiley Online Library on [04/11/2026]. See the Terms and Conditions (https://onlinelibrary.wiley.com/terms-and-conditions) on Wiley Online Library for rules of use; OA articles are governed by the applicable Creative Commons License

And the conductivity of the alloy networks can be estimated to be 2.2×10^3 S cm^{-1}, is given by

$$\sigma_{\mathrm{nw,eq}} = \frac{\sigma_{\mathrm{nw}}}{\eta} = 1/(\eta R d) \tag{3}$$

Slightly lower than the conductivity of SiNi alloy NW array reported in the literature (2×10^4 S cm)$^{-1}$.[36] Furthermore, a piece of SiNi-NS network, with length and width of 1 and 2 cm respectively, was used as flexible conductive electrode to drive 3 LED units, as diagrammed in Figure 3d, assembled upon PI substrate and fixed by silver paste. Under 2 V bias, three LED chips can be easily ignited with passing current of 0.1 mA.

In parallel, the transparency of the SiNi-NS networks was also characterized, when they were transferred onto glass and PI (12.5 µm thick) substrates. As witnessed in Figure 3e,f, the relative transmission of the SiNWs (green) and the SiNi-NW alloy (purple) arrays, excluding the loss due to glass and PI substrates, can be as high as 90% over the full visible light, ranging from 400 to 900 nm, while the overall absolute transmission (all >80%) spectra were provided in Figure S2 (Supporting Information). It is also interesting to note that the transformation of SiNWs into alloy NWs leads to only 3% decrease in the transparency.

In addition, the mechanical stability of the SiNi network, with straight or elastic spring channel geometries, was assessed under gradually increased bending status, which is a critical aspect for practical flexible electronic applications. To this end, the SiNi network on PI substrates were clamped and fixed on a pair of metal stages, as seen **Figure 4**a, which can be programmed and controlled to squeeze, and thus bend, the SiNi-NW@PI (125 µm) sample to desired bending radius. For the initial gap of 3 cm, the smallest bending radius imposed in this work was r = 2 mm (see the lower panels in Figure 4a. As a good reference, the IV characteristics of the straight SiNi network sample was first tested and shown in Figure 4b. It is found that the current drops slowly when the convex bending radius approaches to r = 2 mm, indicating that there are straight SiNi-NWs broken under the enforced bending strain, causing irreversible increase of the overall resistance. This finding highlights that straight SiNi NWs, by themselves, are not good enough channel candidates to form flexible and conductive network. In comparison, the spring SiNi-NW@PI sample demonstrate a rather stable mechanical and electric stability under the same bending conditions, in both convex and concave status, as observed in Figure 4c,d. More importantly, the transport current can remain roughly unchanged for repetitive bending for 1000 cycles to 2 mm radius (see, for example, those shown in Figure 4e,f), with only a tiny fluctuation of ≈2 nA. Also, the fabrication of the NiSi networks and their electric properties are well reproducible, as verified in 8 different samples, with the same size, that showcased only <0.003% current variations (Figure S3, Supporting Information). In addition, the bending testing of the NiSi network sample in both X and Y-axis directions, as shown Figure S4 (Supporting Information), indicate also a good isotropy of the electrical transport properties. These observations emphasize the excellent flexibility of the SiNi-NS

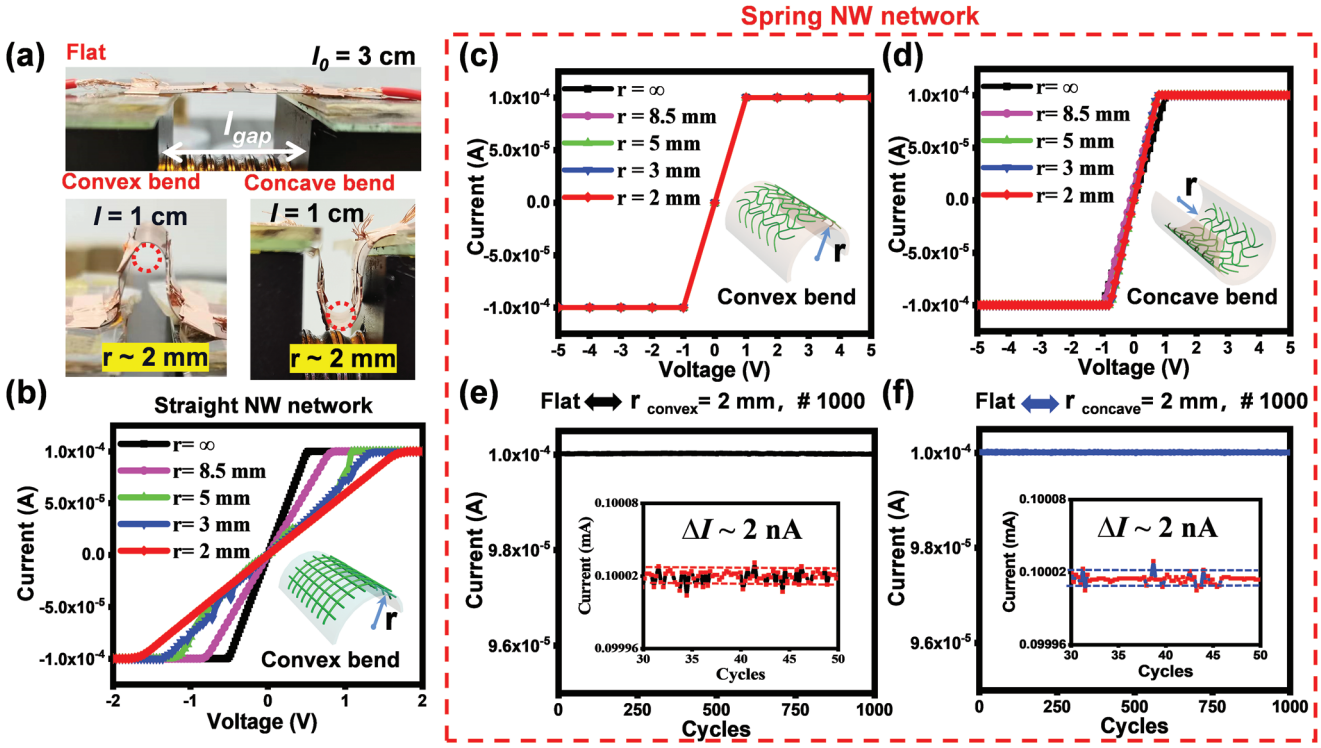


Figure 4. a) Shows the photos of the SiNi alloy network samples upon PI substrate in flat, convex, and concave bending (to radius of ≈2 mm) statues. b) the evolution of the I–V curves of the straight SiNi-NW network under gradually bending radius. In comparison, the I–V curves of the wavy or spring SiNi-NWs under different convex and concave bending radii are provided in c) and d), while the corresponding transport current variations under 3 V bias for repetitive 1000 bending cycles are shown in e) and f), respectively.

© 2023 The Authors. Advanced Electronic Materials published by Wiley-VCH GmbH

2199160x, 2023, 7, Downloaded from https://advanced.onlinelibrary.wiley.com/doi/10.1002/aelm.202201185 by Nanjing University, Wiley Online Library on [04/11/2026]. See the Terms and Conditions (https://onlinelibrary.wiley.com/terms-and-conditions) on Wiley Online Library for rules of use; OA articles are governed by the applicable Creative Commons License

ADVANCED ELECTRONIC MATERIALS
Open Access
www.advelectronicmat.de

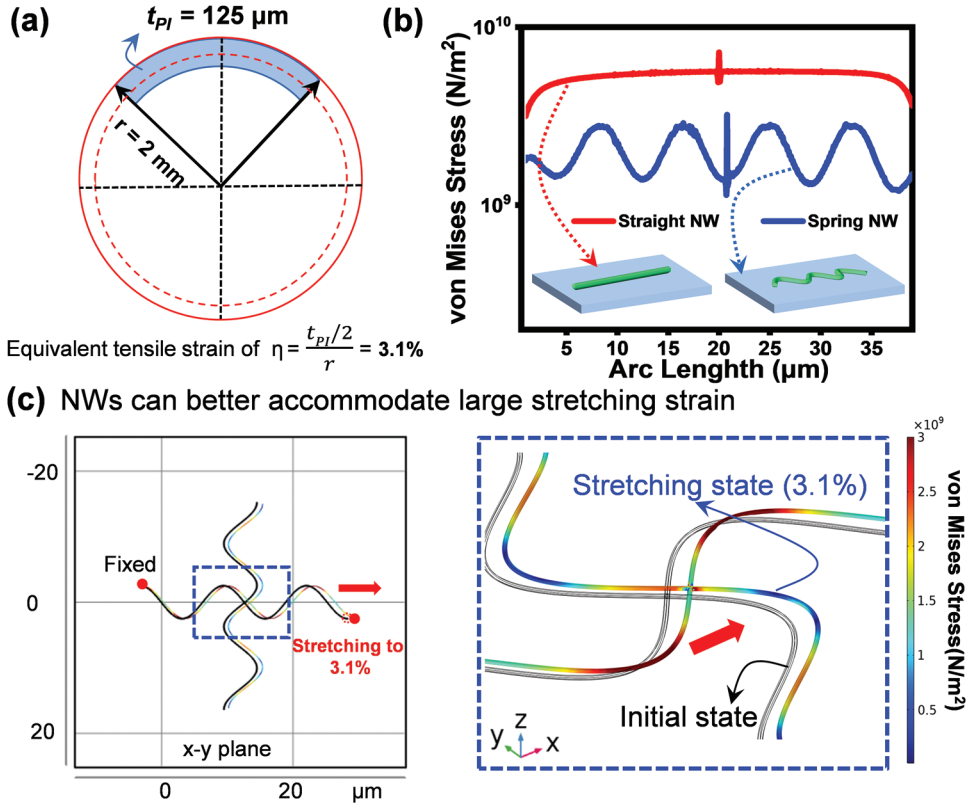


Figure 5. a) Illustrates the conversion of a convex bending status to a surface tensile strain, experienced by the SiNi-NW network upon a flexible PI thin film substrate, leading to an equivalent stretching to 3.1% for convex bending to 2 mm radius. b) The maximal von Mises stresses calculated, by finite element simulation, along a straight or spring-shaped SiNi-NW attached to the stretched PI substrate, while the stress distributions along a pair of cross-linked NW springs are provided in c).

network, thanks to the purposely-designed elastic spring shapes of the slim NW channels, representing a unique capability of the IPSLS guided growth approach. Furthermore, thanks to the stable inorganic NiSi NW networks, the electric transport current remains roughly unchanged over 100 days kept in ambient conditions (Figure S5, Supporting Information).

In order to better understand this improved mechanical stability and the detailed stress distribution of the Si-Ni alloy NWs, a finite element simulation model has been established by using the mechanical module of COMSOL toolkit and as shown in **Figure 5**.

For the convex bending, schematically depicted in Figure 5a, the SiNi-NW network will experience an equivalent tensile stretching to ≈3.1%. The reported straight NW network confined by substrate can only withstand a maximum tensile axial strain of 1.5%,[37] not to mention the more brittle SiNi alloy NWs. On the other hand, the calculated von Mises stresses along a straight or spring-shaped SiNi-NW under 3.1% axial strain are also extracted and presented in Figure 5b, revealing that the spring NW experiences indeed a lower stress (1.1×10^9 to 3.2×10^9 N m^{-2}), compared to its straight counterpart. Though a comprehensive data of the fracture strength of SiNi alloy are not immediately available for us, it is reasonable to assume that SiNi should be more brittle than c-Si, and thus prone to crack under the same stretching. As shown and marked in the Figure 5c, the highest stresses usually appear at the segments parallel to the stretching direction and, most likely, at the crossing points of NWs. Obviously, the elastic spring shape can provide extra space or flexibility for the stretched SiNi NWs to dissipate or convert the stretching strain into local bending, so as to better accommodate the large distortion induced during repetitive bending. In other words, adopting an elastic NW shape is indispensable and rather efficient to integrate the rigid SiNi-NWs to serve as reliable and highly conductive interconnections for future stretchable electronics.

Compared to the flexible network or thin film materials of CNTs,[37,38] graphene film,[39] Au[40] and Ag NWs[41–43] reported in the literature, as summarized in **Table 1**, the orthogonal double-layer stacking formation of conductive network, with designable SiNi-NW/spring channels as demonstrated in this work, has several advantages: 1) first, the precise growth location control of the tiny SiNi-NWs, combined with the high fidelity transferring and alloy network formation technologies, has made it possible to rationally design the NW-layout and batch fabricate optimal cross-linked networks, which are difficult to accomplish via random spin-coating or dispersion approaches. This also enables the best or the most economic use of each constituent NW channels, to seek for sufficient conductivity while leaving as large as possible inter-NW-spacing to achieve a high transparency of the overall thin film. So far, such an orthogonal stacking (with only $N_{stk} = 2$ compared to those typically $N_{stk} \geq 5$) formation of quasi-continuous conductive and transparent net-

© 2023 The Authors. Advanced Electronic Materials published by Wiley-VCH GmbH

2199160x, 2023, 7, Downloaded from https://advanced.onlinelibrary.wiley.com/doi/10.1002/aelm.202201185 by Nanjing University, Wiley Online Library on [04/11/2026]. See the Terms and Conditions (https://onlinelibrary.wiley.com/terms-and-conditions) on Wiley Online Library for rules of use; OA articles are governed by the applicable Creative Commons License

Table 1. Comparison of orderly orthogonal-crossing SiNi-NW network to other flexible and transparent conductive thin films in the literature.

Inorganic conductive channels	Transferred to substrate	Network formation (Arrangement)	Constituent channels	Transmittance & Sheet resistance	Mechanical Testing	Equal tensile	Ref.
Super-aligned CNTs by CVD + metal joints	PVA/PDMS [190 μm]	Laser trimming (Partial orderly)	Straight CNT (≈5 μm wide)	83.4%, 24 Ω sq.$^{-1}$	Bent to 6 mm or stretched to 40% for 1 cycle	2.7%	Ref. [37]
SWCNT grown by CVD	PET (No data)	Aerosol-blowing (Randomly crossed)	Straight CNT	90%, 40 Ω sq.$^{-1}$	Bent to 10 mm for 1 cycle	-	Ref. [38]
Graphene by Ni-assisted growth	PDMS [100 μm]	No network (With random domains)	Multilayer film	80%, 280 Ω sq.$^{-1}$	Bent to 2.3 mm or stretched to 10%	2.2%	Ref. [39]
Bundle-Mesh of Au NWs around pillar array	PET (No data)	Nano-sphere assembly & Etching (Orderly)	Hexagonal bundles with straight Au NWs	92%, 227 Ω sq.$^{-1}$	Bent to 5 mm for 450 cycles	-	Ref. [40]
Bundle-Mesh of Ag NWs	PI [70 μm]	Spray & Spheroidization (Randomly crossed)	Bundle rings with straight Ag NWs	70%, 10 Ω sq.$^{-1}$	Bent to 1.5 mm for 10 000 cycles	2.3%	Ref. [42]
Bundles of Ag NWs	PET [100 μm]	Ice-forming template (Orderly)	Straight Ag NWs in squeezed bundles	91%, 20 Ω sq.$^{-1}$	Bent to 1 cm for 1000 cycles	0.5%	Ref. [23]
Patterned Mesh of Ag NWs	PDMS (No data)	Lithography (Randomly-crossed)	Straight Ag-NWs	No data, 21.7 to 91.3 Ω sq.$^{-1}$	Bent to 5 mm for 100 cycles	-	Ref. [43]
SiNi NWs/springs via IPSLS	PI [125 μm]	Guided growth & alloying (Orderly)	Orthogonally-stacked double SiNi nanosprings	90%, 130 Ω sq.$^{-1}$	Bent to 2 mm for 1000 cycles	3.1%	This work

work has not been demonstrated in previous works; 2) A designable elastic nanospring channel geometry has been adopted in this work to greatly enhance the mechanical stability and electronic durability of the rigid and brittle SiNi alloy NWs in FTC-TF network, which is an unique and indispensable capability for the implementation of future flexible and stretchable electronics. In comparison, most of the Ag or Au NWs, or the CVD VLS-grown metal oxide and Si NWs or CNTs are produced with simple straight shapes, with little geometrical elasticity; 3) The double-layered SiNi-NW network achieves simultaneously an equivalent sheet resistance of 130 Ω sq.$^{-1}$, robust mechanical stability that can sustain repeated bending for 1000 cycles to 2 mm radius and a transparency up to 90%, which represents the best overall combination of the key figure-of-merit parameters (conductivity, flexibility and transparency) for the FTC-TF materials, plus that this alloy NW network can be batch-fabricated economically, via a low temperature (thermal budget up to 350 °C) process that is fully compatible to large area Si-based thin film technology widely used for large-area display and sensor applications.

3. Conclusion

In summary, an orderly orthogonal-crossing and weaving integration of SiNi-NW network, with designable elastic spring shapes and the minimal stacking number of $N_{stk} = 2$, has been demonstrated, for the very first time, upon flexible PI substrate. A low temperature (at 350 °C) alloy formation of SiNi NWs enables a scalable fabrication of highly flexible, transparent and conductive NW-weaving network to serve as ideal FTC-TF materials, with equivalent square resistance of 130 Ω sq.$^{-1}$, excellent mechanical and electric stabilities that can survive 1000 cycles bending to radius of 2 mm, as well as a high transmission of 90% for the wavelengths spanning 400 to 800 nm. These results indicate a new scalable, economic and yet generic network formation or integration strategy of various highly conductive and durable inorganic NWs for future high performance flexible or stretchable electronics, display and sensor applications.

4. Experimental Section

Guiding Edge and Catalyst Formation: The silicon wafers coated with 500 nm SiO_2 were first cleaned by acetone, alcohol, and DI water. The guiding edges with straight and wavy shapes were prepared on SiO_2 surface by using standard photolithography and RIE etching procedures. The etching depth of the guide edge lines were of ≈150 nm. Then, the indium (In) stripes of 35 nm thick and 3 μm wide were patterned and deposited via lithography, thermal evaporation, and standard lift-off procedure.

Growth of SiNW Arrays via IPSLS Strategy: The samples were loaded into PECVD system and then treated by hydrogen plasma for 5 min at 250 °C to remove the native oxide layer, with H_2 flow of 14 SCCM, pressure of 140 Pa and RF power density of 125 mw cm^{-2} RF. After that, a precursor layer of 20 nm amorphous silicon (a-Si) thin film was deposited on the surface of samples at 150 °C (lower than the melting point of indium metal, 157 °C), with SiH_4 gas flow of 5 SCCM, pressure of 20 Pa and RF power density of 60 mW cm^{-2}. In the next step, the substrate temperature was raised to 350 °C and kept in vacuum for 60 min. The In droplets became molten to move along the guiding edge and absorbed the a-Si layer to produce crystalline SiNWs behind. Finally, the remnant a-Si layer was selectively etched off by using H_2 plasma at 120 °C.

Preparation of Conductive SiNi-NW Network: The orthogonal-stacking conductive SiNi network on flexible substrate was fabricated by polymethyl methacrylate (PMMA) assisted transferring and Si-Ni alloying procedures. A PMMA layer with thickness of 200 nm was first coated on the as-grown SiNWs on substrate. Then, the sample was immersed in HF solution (4%) to release the PMMA coated SiNW arrays from the substrates by selectively etching off the underlying SiO_2 layer. After a gently cleaning by DI water, the floated film was picked by flexible polyimide (PI) film (Thickness of 125 or 12.5 μm). In the next step, the film was dipped into acetone to remove the PMMA layer and expose the

© 2023 The Authors. Advanced Electronic Materials published by Wiley-VCH GmbH

2199160x, 2023, 7, Downloaded from https://advanced.onlinelibrary.wiley.com/doi/10.1002/aelm.202201185 by Nanjing University, Wiley Online Library on [04/11/2026]. See the Terms and Conditions (https://onlinelibrary.wiley.com/terms-and-conditions) on Wiley Online Library for rules of use; OA articles are governed by the applicable Creative Commons License

SiNW layer on the flexible substrates. Similarly, the second SiNW layer was transferred and placed in orthogonal direction above the previous SiNW array. The Si-Ni alloying procedure involves first a Ni film (200 nm) deposition by using magnetron sputtering; Then, the sample was loaded into annealing furnace and annealed in 6 mTorr ambient environment at 350 °C for 5 min; Finally, the excess Ni metal was removed in a mixed acid solution (with the volume ratio of V_{H2SO4}:V_{HNO3}: $V_{CH3COOH}$: V_{H2O} = 2:5:5:10).

Finite Element Simulation of the Stress Distribution of SiNi-NW Networks: Stress distribution along the Arc length at the SiNi-NW segment under stretching was modeled and simulated by using COMSOL finite element simulation toolkits. The geometry dimensions (such as the diameter and curvature) of the straight and spring shaped networks were extracted from the SEM observations as shown in Figure 1e, while the material properties of the $SiNi_x$-NW were assumed to be of poly-Si with Young's modulus of 170 GP, Poisson's ratio of 0.28, and density of 2329 kg m^{-3}. The flexible PI substrate was assumed to have a Young's modulus of 5 GPa, and Poisson's ratio of 0.37.

Supporting Information

Supporting Information is available from the Wiley Online Library or from the author.

Acknowledgements

The authors are thankful for financial support received from the National Key Research Program of China under granted no. 92164201 and 61921005, National Natural Science Foundation of China under 11874198, 62104100, and 61974064.

Conflict of Interest

The authors declare no conflict of interest.

Data Availability Statement

The data that support the findings of this study are available in the supplementary material of this article.

Keywords

conductive thin films, flexible electronics, silicide nanowires, transparent thin films

Received: October 28, 2022
Revised: February 27, 2023
Published online: April 28, 2023

[1] B. S. Kim, H. Kwon, H. J. Kwon, J. B. Pyo, J. Oh, S. Y. Hong, J. H. Park, K. Char, J. S. Ha, J. G. Son, S. S. Lee, *Adv. Funct. Mater.* **2020**, *30*, 1910214.
[2] Y. Tang, B. Guo, M. A. Cruz, H. Chen, Q. C. Zhou, Z. F. Lin, F. C. Xu, F. Y. Xu, X. H. Chen, D. J. Cai, B. J. Wiley, J. Y. Kang, *Adv. Sci.* **2022**, *9*, 2201111.
[3] H. K. Kang, S. Jung, S. Jeong, G. J. Kim, K. Lee, *Nat. Commun.* **2015**, *6*, 6503.
[4] Y. Q. Ji, Y. X. Liao, H. H. Li, Y. H. Cai, D. L. Fan, Q. Liu, S. B. Huang, R. J. Zhu, S. Wang, H. Q. Wang, L. Guo, *ACS Appl. Mater. Interfaces* **2022**, *14*, 11971.
[5] H. B. Hu, S. Wang, S. C. Wang, G. W. Liu, T. Cao, Y. Long, *Adv. Funct. Mater.* **2019**, *29*, 1902922.
[6] S. Lee, A. Reuveny, J. Reeder, S. Lee, H. Jin, Q. H. Liu, *Nat. Nanotechnol.* **2016**, *11*, 472.
[7] S. Lee, D. Sasaki, D. Kim, M. Mori, T. Yokota, H. Lee, S. Park, K. Fukuda, M. Sekino, K. Matsuura, T. Shimizu, T. Someya, *Nat. Nanotechnol.* **2019**, *14*, 156.
[8] C. J. C. Clapper, R. E. Erdogan, B. Erdogan, H. Z. Beagi, J. T. A. Everaerts, *Dig. Tech. Pap. - Soc. Inf. Disp. Int. Symp.* **2017**, *48*, 2009.
[9] F. B. Kadumudi, M. Jahanshahi, M. Mehrali, T. G. Zsurzsan, N. Taebnia, M. Hasany, S. Mohanty, A. Knott, B. Godau, M. Akbari, A. D. Pirouz, *Adv. Sci.* **2019**, *6*, 1801241.
[10] Z. F. Li, Y. Liang, Z. C. Zhong, J. Y. Qian, G. J. Liang, K. Zhao, H. X. Shi, S. M. Zhong, Y. Z. Yin, W. J. Tian, *Synth. Met.* **2015**, *210*, 363.
[11] K. J. Kawano, R. Pacios, D. Poplavskyy, J. Nelson, D. D. C. Bradley, J. R. Durrant, *Sol. Energy Mater. Sol. Cells* **2006**, *90*, 3520.
[12] J. L. Sun, Y. Chang, J. Liao, S. L. Chang, S. G. Dai, Y. Y. Shang, C. X. Shan, L. Dong, *Nano Energy* **2022**, *99*, 107392.
[13] Z. Yu, I. R. Perera, T. Daeneke, S. Makuta, Y. Tachibana, J. J. Jasieniak, A. Mishra, P. Bäuerle, L. Spiccia, U. Bach, *NPG Asia Mater.* **2016**, *8*, e305.
[14] J. H. Yun, Y. H. Park, T. S. Bae, S. H. Lee, G. H. Lee, *ACS Appl. Mater. Interfaces* **2013**, *5*, 164.
[15] Q. Dong, Y. Hara, K. T. Vrouwenvelder, K. T. Shin, J. A. Compiano, M. Saif, R. Lopez, *ACS Appl. Mater. Interfaces* **2018**, *10*, 10339.
[16] Y. Leterrier, L. Medico, F. Demarco, J. A. E. Manson, U. Betz, M. F. Escola, M. K. Olsson, F. Atamny, *Thin Solid Films* **2004**, *460*, 156.
[17] K. A. Sierros, N. J. Morris, K. Ramji, D. R. Cairns, *Thin Solid Films* **2009**, *517*, 2590.
[18] D. G. Kuzum, H. Takano, E. Shim, J. C. Reed, H. Juul, A. G. Richardson, J. d. Vries, H. Bink, M. A. Dichter, T. H. Lucas, D. A. Coulter, E. Cubukcu, B. Litt, *Nat. Commun.* **2014**, *5*, 5259.
[19] Y. Y. Chen, Y. Sun, Q. B. Zhu, B. W. Wang, X. Yan, S. Qiu, Q. W. Li, P. X. Hou, C. Liu, D. M. Sun, H. M. Cheng, *Adv. Sci.* **2018**, *5*, 1700965.
[20] P. C. Wang, M. L. Jian, C. Zhang, M. Wu, X. Ling, J. H. Zhang, B. Wei, L. Q. Yang, *Adv. Mater. Interfaces* **2022**, *9*, 2101442.
[21] X. Y. Zhu, Q. Xu, H. K. Li, M. Y. Liu, Z. H. Li, K. Yang, J. W. Zhao, L. Qian, Z. L. Peng, G. M. Zhang, J. J. Yang, F. Wang, D. C. Li, H. B. Lan, *Adv. Mater.* **2019**, *31*, 1902479.
[22] A. Miyamoto, S. Lee, N. S. Lee, M. Mori, N. Matsuhisa, H. Jin, L. Yoda, T. Yokota, A. Itoh, M. Sekino, H. Kawasaki, T. Ebihara, M. Amagai, T. Someya, *Nat. Nanotechnol.* **2017**, *12*, 907.
[23] J. K. Han, J. Yang, W. W. Gao, H. Bai, *Adv. Funct. Mater.* **2021**, *31*, 2010155.
[24] T. Cheng, Y. Z. Zhang, W. Y. Lai, Y. Chen, W. J. Zeng, W. Huang, *J. Mater. Chem. C* **2014**, *2*, 10369.
[25] M. Amjadi, A. Pichitpajongkit, S. Lee, S. Ryu, I. Park, *ACS Nano* **2014**, *8*, 5154.
[26] L. F. Ma, W. Yang, Y. S. Wang, H. Chen, Y. F. Xing, J. C. Wang, *Compos. Sci. Technol.* **2018**, *165*, 190.
[27] L. Yu, P. J. Alet, G. Picardi, P. R. i. Cabarrocas, *Phys. Rev. Lett.* **2009**, *102*, 125501.
[28] Z. G. Xue, M. Sun, T. G. Dong, Z. Q. Tang, Y. L. Zhao, J. Z. Wang, X. L. Wei, L. W. Yu, Q. Chen, J. Xu, Y. Shi, K. J. Chen, P. R. i. Cabarrocas, *Nano Lett.* **2017**, *17*, 7638.
[29] T. G. Dong, Y. Sun, Z. m. Zhu, X. X. Wu, J. Z. Wang, Y. Shi, J. Xu, K. J. Chen, L. W. Yu, *Nano Lett.* **2019**, *19*, 6235.

© 2023 The Authors. Advanced Electronic Materials published by Wiley-VCH GmbH

2199160x, 2023, 7, Downloaded from https://advanced.onlinelibrary.wiley.com/doi/10.1002/aelm.202201185 by Nanjing University, Wiley Online Library on [04/11/2026]. See the Terms and Conditions (https://onlinelibrary.wiley.com/terms-and-conditions) on Wiley Online Library for rules of use; OA articles are governed by the applicable Creative Commons License

[30] H. G. Ma, R. R. Yuan, J. Z. Wang, Y. Shi, J. Xu, K. J. Chen, L. W. Yu, *Nano Lett.* **2020**, *20*, 5072.
[31] Z. G. Liu, J. Yan, H. G. Ma, T. C. Hu, J. Z. Wang, Y. Shi, J. Xu, K. J. Chen, L. W. Yu, *Nano Lett.* **2021**, *21*, 2773.
[32] T. Zhang, R. J. Hu, S. B. Zhang, Z. G. Liu, J. Z. Wang, J. Xu, K. J. Chen, L. W. Yu, *Nano Lett.* **2021**, *21*, 569.
[33] X. P. Song, T. Zhang, L. Wu, R. J. Hu, W. T. Qian, Z. G. Liu, J. Z. Wang, Y. Shi, J. Xu, K. J. Chen, L. W. Yu, *Adv. Sci.* **2022**, *9*, 2105623.
[34] S. B. Zhang, T. Zhang, Z. G. Liu, J. Z. Wang, L. W. Yu, J. Xu, K. J. Chen, P. R. i. Cabarrocas, *Nano Energy* **2021**, *86*, 106121.
[35] X. L. Sun, T. Zhang, J. Z. Wang, F. Yang, L. Xu, J. Xu, Y. Shi, K. J. Chen, P. R. i. Cabarrocasc, L. W. Yu, *Nano Energy* **2018**, *53*, 83.
[36] R. R. Yuan, W. T. Qian, Z. G. Liu, J. Z. Wang, J. Xu, K. J. Chen, L. W. Yu, *Small* **2021**, *18*, 2104690.
[37] K. Liu, Y. H. Sun, P. Liu, X. Y. Lin, S. S. Fan, K. L. Jiang, *Adv. Funct. Mater.* **2011**, *21*, 2721.
[38] Q. Zhang, W. Y. Zhou, X. G. Xia, K. W. Li, N. Zhang, Y. C. Wang, Z. J. Xiao, Q. X. Fan, E. I. Kauppinen, S. S. Xie, *Adv. Mater.* **2020**, *32*, 2004277.
[39] K. S. Kim, Y. Z. H. Jang, S. Y. Lee, J. M. Kim, K. S. Kim, J. H. Ahn, P. Kim, J. Y. Choi, B. H. Hong, *Nat. Commun.* **2009**, *457*, 706.
[40] J. H. M. Maurer, L. G. García, B. Reiser, I. Kanelidis, T. Kraus, *Nano Lett.* **2016**, *16*, 2921.
[41] Y. Yang, J. L. Wang, L. Liu, Z. H. Wang, J. W. Liu, S. H. Yu, *Nanoscale* **2017**, *9*, 52.
[42] B. W. Sun, R. X. Xu, X. Han, J. Xu, W. Hong, Y. M. Xu, Z. W. Fu, H. Zhu, X. Sun, J. X. Wang, P. Cui, J. J. Chang, J. Q. Xiong, K. Qian, *Npj Flex Electron* **2022**, *6*, 48.
[43] Y. Ahn, H. Lee, D. Lee, Y. Lee, *ACS Appl. Mater. Interfaces* **2014**, *6*, 18401.

© 2023 The Authors. Advanced Electronic Materials published by Wiley-VCH GmbH

2199160x, 2023, 7, Downloaded from https://advanced.onlinelibrary.wiley.com/doi/10.1002/aelm.202201185 by Nanjing University, Wiley Online Library on [04/11/2026]. See the Terms and Conditions (https://onlinelibrary.wiley.com/terms-and-conditions) on Wiley Online Library for rules of use; OA articles are governed by the applicable Creative Commons License